Linking the Surface and Subsurface in River Deltas - Part 2: Relating Subsurface Geometry to Groundwater Flow Behavior

Zhongyuan Xu[1], Jayaram Hariharan[2], Paola Passalacqua[2], Elisabeth Steel[3], Chris Paola[4], Holly A. Michael[1,5*]

[1]Department of Earth Sciences, University of Delaware, Newark, Delaware, USA

[2]Department of Civil, Architectural and Environmental Engineering and Center for Water and the Environment, University of Texas at Austin, Austin, TX, USA

[3]Department of Geological Sciences and Geological Engineering, Queen's University, Kingston, Ontario, Canada

[4]Department of Earth and Environmental Sciences, University of Minnesota, Minneapolis, Minnesota, USA

[5]Department of Civil and Environmental Engineering, University of Delaware, Newark, Delaware, USA

Corresponding author: Holly A. Michael (hmichael@udel.edu)

Key Points:

- In delta systems, net-to-gross ratio metrics highly correlate with horizontal flow, metrics of vertical connections highly correlate with vertical flow.
- Deltas with higher sand input have lower horizontal and vertical normalized dynamic connectivity.
- Deltas with higher SLR rates have higher horizontal normalized dynamic connectivity, while SLR has no obvious effect on vertical dynamic connectivity.

Abstract

Understanding subsurface structure and groundwater flow in deltaic aquifers is essential to evaluating the vulnerability of groundwater resources in delta systems. Deltaic aquifers contain coarse-grained paleo-channels that preserve a record of former surface river channels as well as fine-grained floodplain deposits. The distribution of these deposits and how they are interconnected control groundwater flow and contaminant transport. In this work, we link depositional environments of deltaic aquifers to stratigraphic (static) and flow and transport (dynamic) connectivity metrics. Numerical models of deltaic stratigraphy were generated using a reduced-complexity numerical model (DeltaRCM) with different input sand fractions (ISF) and rates of sea-level rise (SLR). The groundwater flow and advective transport behavior of these deltas were simulated using MODFLOW and MODPATH. By comparing the static and dynamic metrics calculated from these numerical models, we show that groundwater behavior can be predicted by particular aspects of the subsurface architecture, and that horizontal and vertical connectivity display different characteristics. We also evaluate relationships between connectivity metrics and two environmental controls on delta evolution: ISF and SLR rate. The results show that geologic setting strongly influences both static and dynamic connectivity in different directions. These results provide insights into quantitatively differentiated subsurface hydraulic behavior between deltas formed under different external forcing (ISF and SLR rate) and they are a potential link in using information from delta surface networks and depositional history to predict vulnerability to aquifer contamination.

Plain Language Summary

Geologic structure and groundwater flow behaviors influence groundwater resources in delta plains. In deltaic aquifers, channel structures were created by past surface rivers. These channels in the subsurface are ‘fast-travel’ pathways for groundwater flow and contaminant transport. We created synthetic delta structures with a numerical model and then simulated groundwater flow through them in order to tie geologic structure to groundwater flow behavior. By using many different models, we investigate how structure and flow relate, and how the subsurface geology and groundwater system are affected by different sediment inputs and sea-level rise rates. The findings will help us better manage delta groundwater resources and provide an opportunity to predict groundwater contamination from surface characteristics.

1 Introduction

Nearly half a billion people inhabit delta regions across the world and more than 40% of fresh water flows through deltas before entering global oceans (Syvitski and Saito, 2007). In many delta regions, groundwater is the primary source for drinking and irrigation (Shamsudduha et al., 2011). However, the groundwater resources of deltas are threatened by several factors, such as over-pumping, seawater intrusion and anthropogenic and geogenic contamination (Syvitski et al., 2009; Tessler et al., 2015; Overeem & Syvitski, 2009; Wada et al., 2010). Efforts to sustainably manage these resources and reduce vulnerability to contamination must consider both hydrology and subsurface structure (e.g., Michael and Khan, 2016; Khan et al., 2016). However, the complexity of delta architecture makes inference of structure from direct observations prohibitive. Improving understanding of the linkages between external forcings that can be observed or inferred, subsurface structure, and groundwater flow and contaminant transport behaviors will improve our ability to manage delta aquifers and preserve water resources for future generations.

The sedimentary structural controls on flow and transport have been demonstrated in aquifers through numerical modeling (Wen & Gomez-Hernandez, 1998; Zinn & Harvey, 2003; Dagan et al., 2003; Jankovic et al., 2017). Due to the difficulty in explicitly representing deltaic heterogeneity over large scales, parameters are often upscaled in regional models. For example, homogeneous and anisotropic hydraulic conductivity (*K*) were used to model the Colorado River Delta (Feirstein et al., 2008; Mohammed et al., 2017), the Bengal Delta (Michael & Voss, 2009), and the Mississippi Delta (Barlow & Clark, 2011;). On smaller scales, heterogeneity and subsurface structure have been incorporated in groundwater flow and solute transport models. Grain-size heterogeneity and clay beds have been incorporated into models of the Mekong Delta (Erban et al., 2013) and the Bengal Delta (Hoque et al., 2017). Additionally, palaeohydrology has been shown to control 3D structure and groundwater salinity in the Nile Delta (van Engelen, 2019) and salinity traps and arsenic levels in the Red River Delta (Larsen et al., 2017). Michael and Khan (2016) and Khan et al. (2016) showed that heterogeneity-induced preferential flow plays an important role in aquifer vulnerability to contaminant migration in the Bengal Delta. Numerous sedimentological studies have demonstrated the prevalence of sandy paleo-channels in deltaic stratigraphy (Straub et al., 2009; Miall, 2014; Bhattacharyya et al., 2015), which are expected to affect the subsurface connectivity. Kolker et al. (2013) demonstrated that these paleo-channels serve as conduits for preferential flow in the Mississippi River Delta. Sawyer et al. (2015) showed that surface water – groundwater interaction was influenced by channel connectivity and sediment grain size. Rao et al. (2015) showed the importance of a single paleo-channel on coastal groundwater development in deltaic aquifers.

Though the effects of deltaic heterogeneity on groundwater flow and solute transport have been clearly demonstrated on multiple scales, the nature of characteristic delta channel networks has not been fully considered. Connected channels on the delta surface distribute water and sediments, with directionality determined by the hydrology and geology of the system (Shaw, 2013; Hiatt & Passalacqua, 2015; Reitz et al., 2015). The channels move across the delta surface, through avulsion or migration, due to both external and internal forcings, such as tides, sea-level rise, sediment grain size and river flow rate (Heller et al., 2001; Sheets et al., 2002; Kim et al., 2006). Subsurface paleo-channels are then created through burial and translation into the subsurface of the surface channel network (Liang et al., 2016a), and their subsurface connectivity structure can be tied to various surface conditions (Hariharan et al., submitted). The nature of the connectedness of coarse-grained channels and fine-grained matrix controls the flow of subsurface fluids, potentially resulting in highly preferential flow (Krishnan and Journel, 2003; Kolker et al., 2013).

To better understand the subsurface channel connection and corresponding flow behavior in deltaic aquifers, the concept of connectivity is used in this study. Connectivity represents one of the fundamental properties of a system; it relates to heterogeneity and reflects the nature of connected geologic features that have a substantial impact on flow and transport (Dagan, 1986; Gelhar, 1986; Kundby and Carrera, 2006). A number of studies have shown that structural connections in a heterogeneous system is a better conceptualization for predicting dynamic behavior than two-point statistics. For example, Sanchez-Vila et al. (1996) noted that systems with high-*K* connections have a larger effective *K* than multi-Gaussian fields with similar *K* variations. Madden (1983) and de Marsily (1985) discussed the importance of connectivity on flow and transport in fractured rock systems. Zinn & Harvey (2003) revealed the differences in dynamic behavior among high-*K* connected systems, multi-Gaussian systems and low-*K* connected systems. They showed that the effective conductivity is higher and solute transport is faster in high-*K* connected fields.

Despite the importance of connectivity to flow and transport, its definition and measurement are not straightforward (Kundby and Carrera, 2005; 2006; Western et al., 2001). Thus, a variety of quantitative metrics of connectivity have been developed. In general, connectivity metrics can be divided into two groups: static and dynamic (Renard & Allard, 2013). Static connectivity metrics quantify the intrinsic properties of geologic media that connect spatially, such as permeability or porosity. Many studies simplify the heterogeneous geologic field to a binary system, resulting in more-permeable or less-permeable 'geobodies' (Western et al., 2001; Larue & Hovadik, 2006; Kundby et al., 2006). Dynamic connectivity metrics quantify the flow and solute transport behavior affected by connected structures, particularly preferential flow and fast solute transport. These metrics depend not only on the geologic system, but also on the hydraulic gradient and aquifer geometry. Static and dynamic metrics are related, but the relationship is complex and not well defined. Bianchi et al. (2011) showed similar variations in static and dynamic metrics among different statistical models. Renard & Allard (2013) reviewed the relationship between effective *K* and the proportion of high-*K* zones within an aquifer (net-to-gross ratio), and proposed that effective *K* is not a simple function of net-to-gross ratio but is also controlled by continuity, low-*K* barriers, and percolation status.

In deltaic aquifers, static connectivity and external forcings may be more easily inferred than dynamic flow and transport behaviors, and we expect that these are related, since delta channel distributions and morphology are sensitive to variations in the external forcings, such as sand fraction and the rate of sea-level rise (Liang et al. 2016a; 2016b). Therefore, in this study, we investigate (1) the relationship between subsurface static and dynamic connectivity within numerically generated deltas, and (2) the influence of input sand fraction and rates of sea-level rise on subsurface static and dynamic metrics. In a companion paper (Hariharan et al., submitted), we explore the relationship between surface metrics and static subsurface metrics.

2 Methods

2.1 Process-based modeling

Numerical models of deltaic aquifers were produced with DeltaRCM (Liang et al., 2015a), a cellular, reduced-complexity morphodynamic model based on a set of physical rules. These rules regulate the transport of water and sediment particles through the system in a Lagrangian fashion using a weighted random walk. DeltaRCM can resolve a wide range of channel dynamics and reproduce important processes in delta generation. The detailed numerical implementation is extensively described in Liang et al. (2015a; 2015b), and is not repeated here.

Conceptually, we considered one river inlet in a coastal area. Surface and subsurface channel networks conform to the general delta network distribution: sparse main channels in the upstream region, and multiple, complex distributaries downstream (Figure 1a). Sediment is transported by these branching river channels to build the delta. In DeltaRCM, the aquifer was discretized into rectangular cells with dimension 50 m × 50 m × 5 cm. The size of each model is different, so they have different numbers of cells. After sediment deposition, the sand content in each cell is recorded, ranging from 0 (no sand at all – pure mud) to 1 (pure sand).

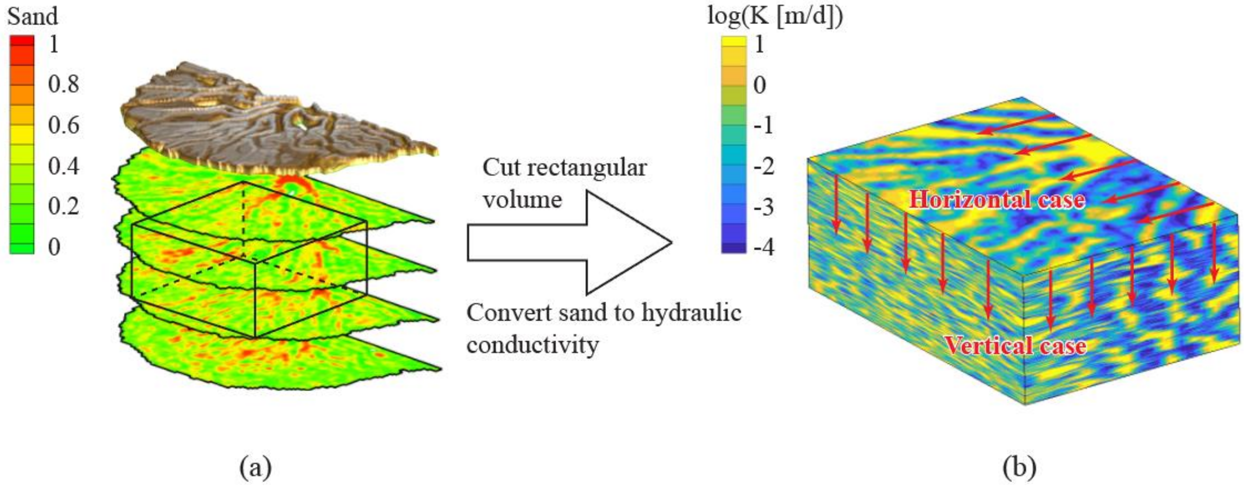

Figure 1. The model of delta stratigraphy used in this study. (a) the delta generated numerically by DeltaRCM with a surface channel network and subsurface channel distribution. (b) the rectangular volume extracted from (a) for groundwater modeling. Red arrows are direction of flow in the horizontal and vertical cases for numerical groundwater flow simulations, K is hydraulic conductivity. The conversion of the DeltaRCM realizations to groundwater models is detailed in Text S2 in the Supporting Information.

A set of 240 deltas were generated using DeltaRCM, these realizations were randomly generated based on weighted random walks (Liang et al., 2015a). Two variations in external conditions were considered and analyzed in this study, input sand fraction (ISF) and rate of sea-level rise (SLR), other physical parameters and basin geometry were the same as those in Liang et al. (2016a) as this parameter set was validated against real and experimental deltas. The ISF is the sand fraction input at the inlet boundary, which controls the total sand fraction in the aquifer, though the actual sand fraction in the preserved stratigraphy depends on fractionation between various depositional elements (e.g. channel vs floodplain). ISF also strongly influences the sand content of each cell and the channel distribution in the system, for example sandy deltas have higher channel mobility and more active distributaries (Liang et al., 2016a). We used three ISFs in this study: 30%, 50%, and 70%, to span a range of values while avoiding extremes which tend to homogeneity. The rate of SLR is another critical component of delta evolution. The current average rate of SLR is around 3.3 mm/y (Cazenave et al., 2014), and before the mid-Holocene when deltas rapidly built, this rate was ~10 - 20 mm/y (Goodbred et al., 2003; Spratt & Lisiecki, 2016). Increasing the SLR rate results in more channel distributaries and a thicker but narrower delta (Liang et al., 2016a). We used a wide range of SLR rate, from 0 to 60 mm/y. Only DeltaRCM simulations run with high SLR rates (40, 50, 60 mm/y) are able to generate models with enough stratigraphy to span our criterion of at least 10 channel heights within a reasonable timeframe. In order to incorporate the full range of SLR rate in our analysis (0, 5, 10, 20, 30 mm/y), we developed a method to stitch together multiple low SLR rate models to obtain an aquifer of sufficient thickness, as explained in Hariharan et al. (submitted). We tested the stitching method to ensure it does not strongly influence the connectivity in the system (Text S1).

Overall, the five scenarios from 0 to 30 mm/y are stitched models, and the three from 40 to 60 mm/y are raw (unstitched) models.

2.2 Groundwater modeling

To create models with some degree of spatial statistical stationarity, and for convenient computation of connectivity metrics and assignment of flow boundaries, we extracted a rectangular volume from the full DeltaRCM model (Figure 1). The grid of the groundwater model is the same as that of the stratigraphic model. Because the size of the simulated deltas varies under different SLR rates, the strategy of box cutting is dependent on the delta size and is designed to maintain a consistent sampled portion of the delta among different SLR rates (Text S2, Figure S1). Therefore, groundwater models under different SLR rates have different dimensions. The depth of low SLR rate models was 25 m after stitching, and the depth of high SLR rate models was variable. There was also a small difference in the size of models with the same SLR rates because deltas were generated randomly. The rough dimensions of the groundwater models for each SLR rate is shown in Figure S2.

The sand content in each model cell was converted to *K*. The *K* values of pure sand and pure mud were set as 1e-4 m/s and 1e-9 m/s, respectively. The *K* of each cell was calculated based on the geometric mean of sand content value (Text S2). The relationship of *K* and sand content is presented in Figure S3 and explained in Text S2 in the SI.

We simulated steady-state groundwater flow with MODFLOW (Harbaugh et al., 2005), considering two cases: horizontal and vertical (Figure 2). In the horizontal case, h_1 = 1 m was assigned to the face of the inlet, h_2 = 0 m was assigned to the face at the seaside, and no-flow boundary conditions were imposed on the other four faces. In the vertical case, h_1 = 1 m and h_2 = 0 m were assigned to the top and bottom faces, respectively, and the other four faces were no-flow boundaries. The particle travel times in the simulated flow field were calculated with MODPATH (Pollock, 2016). More than 20,000 particles were evenly distributed across the upstream face in the horizontal case with at least 1 particle in each cell, and more than 12,000 particles were used in the vertical case with at least 5 particles in each cell. Only advective transport is considered in this study, and the effects of mechanical dispersion and molecular diffusion are ignored. Effective conductivity and travel times calculated in MODFLOW and MODPATH are used to calculate connectivity metrics.

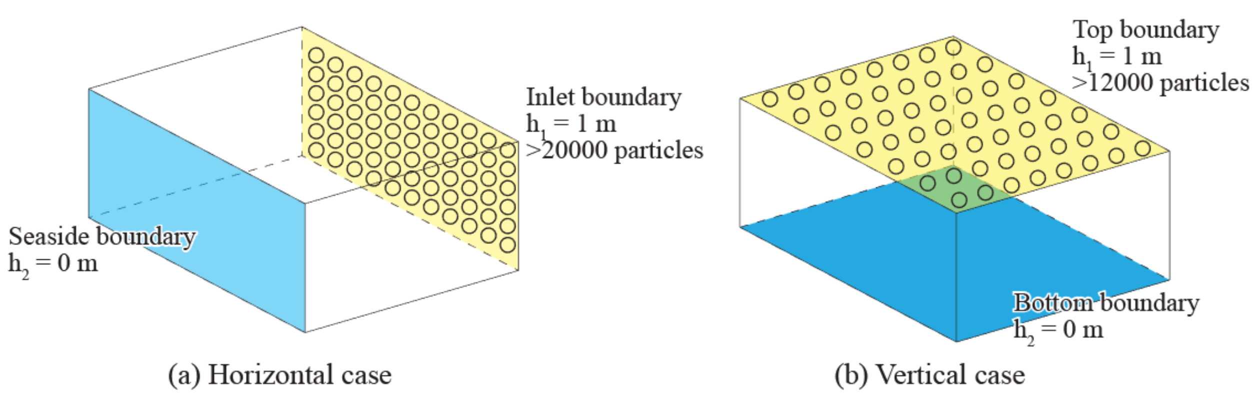

Figure 2. Boundary conditions of horizontal and vertical cases. Yellow face is the higher-head boundary, blue is the lower-head boundary, no-color faces are no-flow boundaries.

2.3 Connectivity metrics

Ideal connectivity metrics are those that can be easily measured and can sufficiently represent the spatial distribution of parameters and dynamic behaviors. Static connectivity metrics were calculated based on the spatial characteristics of the geologic model in 3D and 2D sections, and dynamic connectivity metrics were calculated based on the results of the groundwater flow simulation. We calculated 30 metrics to analyze correlations between static and dynamic connectivity. Only those metrics that proved to be significantly correlated are shown below (Tables 1 & 2). Among them, we selected 12 connectivity metrics from previous studies (Kundby and Carrera, 2005; 2006; Renard & Allard, 2013) and we formulated 18 other metrics for deltaic characteristics. In the companion paper, Hariharan et al. (submitted), probability distributions were used to compare surface and subsurface static metrics. Here, we use single average values of the static metrics in order to better correlate them to typical dynamic metrics.

Static connectivity metrics capture spatial parameter distributions and channel connectedness. Because it is more straightforward to quantify connectivity in a binary system, the K field was converted to binary using a threshold of 0.8 sand content. The basis for this threshold is discussed in Text S3, and we note that the threshold choice had little effect on the results, as the original distribution was strongly bimodal (Figure S4). A group of connected cells with K values equal to or larger than the threshold are defined as a *geobody* (Larue & Hovadik, 2006; Hovadik & Larue, 2007; Stauffer & Aharony, 2014), and a geobody that connects opposite boundaries is designated as a *percolated path* (Figure S5). To avoid bias related to the total sand fraction in the system and to specifically target the effect of spatial connections, we normalized the volume of the largest geobody and percolated path by sand volume (0.8). We then calculated normalized volumes in 2D planes with different directions. These metrics are *Horizontal*, *Strike,* and *Dip section connectivity*, and *Horizontal, Strike,* and *Dip section percolated path ratio* (Table 1). Another set of metrics is based on sampling a *core*, defined as a 1D, vertical column in the system (Figure S6). We calculated the arithmetic mean of sand content of each core and converted the 3D box to a map of vertically-averaged sand content (Figure S6), which reflects channel stacking patterns and vertical connections. Two static metrics were derived from this map, *Highest core sand fraction* and *Fraction of high sand cores* (Table 1). We classified the static metrics into two orders (Table 1). First-order metrics reflect bulk properties, essentially the net-to-gross ratio. Second-order metrics reflect the spatial connection of high-K faces. These properties were calculated on the entire extracted domain, and also locally by dividing the domain into three regions. Regions 1, 2, and 3 are the closest, intermediate and farthest from the delta source, respectively (Figure S7), reflecting differences in channel distributions from upstream to downstream (Table 1).

Table 1. Static metric definitions. 1st order static metrics reflect bulk properties and overall net-to-gross ratio, 2nd order static metrics show the spatial distribution. The definition of geobody and percolated path are in Figure S5, the definition of core and averaged sand content map is in Figure S6.

Metric	**Order**	**Definition**
Sand Fraction	1	Average sand content of all cells in the system
K_G [L/T]	1	Geometric mean of hydraulic conductivity (K) of all the cells
Average Geobody Volume [L^3]	2	Average volume of geobodies
Horizontal Section Connectivity [0]	2	Arithmetic mean over horizontal sections of the ratio of the largest geobody to the total area of geobodies in each section.
Strike Section Connectivity [0]	2	Arithmetic mean over strike vertical sections of the ratio of the largest geobody to the total area of geobodies in each section.
Dip Section Connectivity [0]	2	Arithmetic mean over dip vertical sections of the ratio of the largest geobody to the total area of geobodies in each section.
Horizontal Section Percolated Path ratio [0]	2	Arithmetic mean over horizontal sections of the ratio of percolated path geobodies to the total summed area of geobodies in each section.
Strike Section Percolated Path ratio [0]	2	Arithmetic mean over strike vertical sections of the ratio of percolated paths to total summed area of geobodies in each section.
Dip Section Percolated Path ratio [0]	2	Arithmetic mean over dip vertical sections of the ratio of percolated paths to total summed area of geobodies in each section.
Highest Core Sand Fraction [0]	2	The highest sand fraction of any core in the domain
Fraction of High Sand Cores [0]	2	The number of vertical columns (cores) with greater than 0.8 sand content divided by the total number of cores.
Local metrics	/	Static metrics above calculated in Region 1, 2 and 3 (Figure S7)

Dynamic connectivity metrics (Table 2) are used to measure the flow and advective transport behavior. These metrics were derived from the results of numerical groundwater flow modeling and particle tracking in the horizontal and vertical directions, designed to target preferential flow behavior in particular. The simplest and most widely used metric is effective hydraulic conductivity (K_{eff}) (Guswa & Freyberg, 2002), calculated by simulating horizontal and vertical flow through each model to obtain specific discharge for a given gradient, then back-calculating K_{eff} by Darcy's law. According to Matheron (1967), K_{eff} is equal to the geometric mean of K (K_G) for an isotropic, multi-Gaussian field. Thus, the ratio $Keff\,/K_G$ is widely used as a normalized connectivity indicator measuring overall flow behavior normalized, in effect, by net-to-gross ratio (Knudby & Carrera, 2005; Zarlenga et al., 2018). For advective transport, Knudby & Carrera (2005) proposed the ratio of early arrival time to average arrival time (T_a/T_5) as an advective transport-normalized connectivity metric derived from breakthrough curves; it represents preferential flow normalized by overall flow behavior. K_{eff}/K_G and T_a/T_5 have been widely used as dynamic connectivity metrics in previous studies (Knudby & Carrera, 2005; Zinn & Harvey, 2003; Jankovic et al., 2017; Le Goc et al., 2010; Frippiat et al., 2009). In addition, *preferential discharge* measures the importance of preferential flow in the total discharge; it is defined as the fraction of discharge at the exit locations of the first 5% of particles to arrive relative to total discharge (Bianchi et al., 2011).

Table 2. The definition of dynamic metrics. All metrics were calculated in both horizontal and vertical directions.

Metric	Order	Definition
K_{eff} [L/T]	Overall flow	Effective *K* calculated by Darcy's Law
K_{eff}/K_G [-]	Overall flow / net-to-gross	Effective *K* normalized by geometric mean of *K*. This metric indicates overall flow normalized by a 1st order static metric.
L/T_a[L/T]	Overall flow	Inverse of geometric mean of travel time of all particles tracked from one constant head boundary to the opposite boundary, *L* is the distance between boundaries
L/T_5 [L/T]	Preferential flow	Inverse of 5th percentile of travel time of particles tracked from one constant head boundary to the opposite boundary, *L* is the distance between boundaries
T_a/T_5 [-]	Preferential flow / overall flow	5th percentile of travel time normalized by geometric mean of travel times. This metric indicates preferential flow normalized by overall flow.
Preferential Discharge [-]	Preferential flow	The fraction of discharge at the exit locations of fast flow paths (first 5% to arrive) to total discharge.

3 Results

3.1 Relationships between static and dynamic metrics

The correlations between static and dynamic metrics provide insights into the controls of sedimentary architecture on groundwater flow and advective transport in deltaic aquifers. A high correlation between a static and dynamic metric suggests that the given dynamic metric can be predicted with the static metric. These correlations are useful because static metrics are generally more easily measured than dynamic metrics. We calculated Pearson correlation coefficients for each pair of metrics across the 240 model simulations – 10 realizations each for 3 ISF and 8 SLR rates – 24 combinations of each pair of metrics. We consider a static metric to be predictive of a dynamic metric if 12 out of the 24 combinations are significantly correlated; these are shown in Table 3. Correlations for all static-dynamic metric pairs are given in Table S2.

Horizontally, 1st-order static metrics tend to be correlated with overall flow behavior (K_{eff}, K_{eff}/K_G, and L/T_a). For example, *sand fraction* and K_G are highly correlated with K_{eff} and K_{eff}/K_G (Table 3). Most of the P-values are less than 0.01, which indicates a strong correlation between the static metrics and overall flow. This is because the delta is a highly connected system horizontally, so the sand fraction exerts a primary control on the percolated paths and connected geobodies, which in turn drives flow behavior. However, none of the static metrics correlate with transport metrics to a high significance level. *Horizontal section percolated path ratio* is the most predictive static metric for preferential flow (L/T_5) (Table 3). In addition, the left panel of

Figure 3 shows that most of the preferential flow follows the high-sand clusters in the horizontal direction, which also indicates that the horizontal sand distribution controls the flow behavior.

Table 3. Highly correlated static and dynamic metrics. Each pair of static-dynamic metrics has 21 correlations, they are listed in this table if more than 10 correlations are significant. The significant correlations are based on the P-values in Pearson Correlation.

Static metrics	Dynamic metrics	# of p-values⩽ 0.05	# of p-values ⩽ 0.01
Sand Fraction	Horizontal K_{eff}	21	14
Sand Fraction	Horizontal K_{eff}/K_G	20	18
K_G	Horizontal Keff	20	14
K_G	Horizontal K_{eff}/K_G	22	20
Average Geobody Volume	Horizontal K_{eff}	15	9
Horizontal Section Connectivity	Horizontal K_{eff}	13	6
Horizontal Section Connectivity	Horizontal K_{eff}/K_G	12	5
Horizontal Section Percolated Path Ratio	Horizontal K_{eff}	16	8
Horizontal Section Percolated Path Ratio	Horizontal T_5	12	4
Dip Section Percolated Path Ratio	Vertical K_{eff}	12	5
Highest Core Sand Fraction	Vertical K_{eff}	13	5
Highest Core Sand Fraction	Vertical K_{eff}/K_G	12	5
Highest Core Sand Fraction	Vertical T_5	13	6
Fraction of High Sand Core	Vertical K_{eff}	12	4
Fraction of High Sand Core in Region 1	Vertical K_{eff}	13	4
Fraction of High Sand Core in Region 1	Vertical T_5	12	5

In the vertical direction, the flow paths are more tortuous, and preferential flow follows sand bodies connected by channel stacking (Figure 3, right panel). Dynamic connectivity metrics such as K_{eff} are best predicted by static metrics that reflect vertical spatial connections and channel stacking patterns, such as *dip section percolated path ratio*, *fraction of high sand core,* and *highest core sand fraction* (Table 3). Additionally, *highest core sand fraction,* which represents the stability of channel stacking, is highly predictive of vertical preferential flow (L/T_5) with 13 significant correlations (Table 3). However, most of the p-values for the static-dynamic correlations are larger than 0.01, which indicates weaker correlations in the vertical direction compared to the horizontal direction. The system is less connected in the vertical direction because channels are inherently horizontal features, transporting sand and water basinward and depositing horizontally-connected sandbodies. High-sand connections between the top and bottom boundaries (i.e. vertical connectivity) are highly sensitive to channel stacking driven by channel migration and avulsion, which depends on ISF and rate of SLR (Section 3.2 & 3.3).

Another characteristic of vertical groundwater flow is that preferential flow is concentrated in the upstream portion, near the sediment source (Figure 3 b&d), where lateral channel migration is low and channels have a tendency to stack vertically. Thus, local metrics in Region 1 play a more important role in predicting vertical flow than in Regions 2 and 3 (Table S2; Figure S7). For example, *fraction of high sand core* in Region 1 is significantly correlated with *vertical* K_{eff} and *vertical* L/T_5 (Table 3), but the correlation is not strong for the *fraction of high sand core* in Regions 2 and 3 (Table S2).

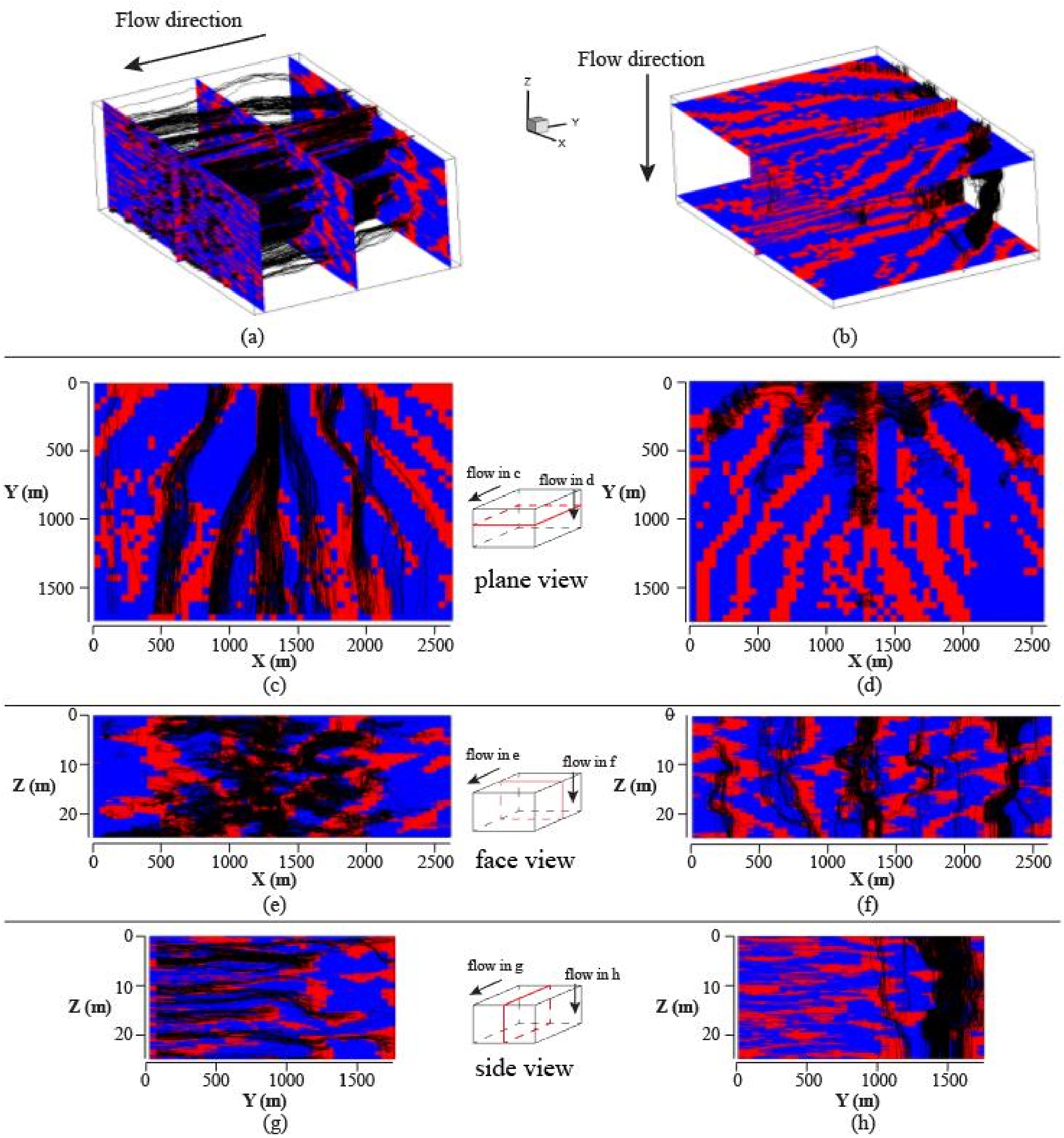

Figure 3. Sand distribution and preferential flow lines for one realization of a model with ISF=30% and SLR rate=40 mm/y. Red areas are high-sand clusters and black lines are flow paths of the 5% fastest particles. From top to bottom are 3D view, plan view, face view, and side view. Left is horizontal flow simulation, right is vertical flow simulation.

3.2 The effect of input sand fraction on connectivity

Input Sand Fraction (ISF) is the total amount of sand initially put into the system. ISF directly determines how much sand is in the delta as a whole, with some variability due extraction of the sub-domain. Sandy deltas tend to have greater channel mobility and shallower channel depth, which cause more variable channel stacking and therefore more variable vertical connectivity. Muddy deltas tend to display less mobile and deeper channels, leading to more stable channels and more consistent vertical stacking (Liang et al., 2016a). Realizations of 0 and 40 mm/y SLR rates shown in Figure 4 indicate the effect of ISF on stitched and non-stitched models. The actual sand fraction of models is higher than the corresponding ISF due to model cutting (Text S2). In general, the impact of ISF on connectivity metrics is similar in models with SLR rates from 0 mm/y to 60mm/y (Figure S8-S10). Two dynamic normalized connectivity metrics, K_{eff}/K_G and T_a/T_5, are analyzed in this section.

In the horizontal direction, non-normalized static and dynamic metrics generally increased with increasing ISF due to higher overall K values (Figure S9 a,d,e). However, the normalized ratios of K_{eff}/K_G and T_a/T_5 decreased from 100 to less than 20 with increasing sand fraction in both low SLR and high SLR rates (Figure 4 a&b and Figure S9 b&f). This indicates that the channel distributions with less sand input remain well connected; a larger sand input only increases the width of preserved channels, which effectively makes it more like a homogeneous system. K_{eff}/K_G nonlinearly decreases with ISF (Figure 4a) because K_G increases more with ISF than K_{eff} does. This is because the horizontal system is always percolated by sand-rich channels, so the overall horizontal flow behavior is relatively insensitive to the variation of sand fraction. T_a/T_5 also shows an inverse trend with sand fraction (Figure 4b). Similar to K_{eff}/K_G, preferential flow (L/T_5) is more controlled by the presence of percolated channels than overall flow (L/T_a). Thus preferential flow changes less than overall flow after adding more sand into system, the ratio of T_a/T_5 decreases with increasing sand input. Nearly 30% of water discharged through the fast flow exit locations (where the fastest 5% of tracked particles exited the model) in 30% ISF models, while this percentage decreased to 10% with more sand input (Figure S9c). This implies that preferential flow is not a primary control on horizontal flow and transport in percolated deltaic aquifers. The presence of many relatively efficient paths means that the tail of highly efficient ones does not have a strong influence.

In the vertical direction, the ratios of K_{eff}/K_G and T_a/T_5 are orders of magnitude smaller than in the horizontal case (Figure 4 c&d). In particular, $K_{eff}/K_G < 1$, which indicates that the system is not well connected vertically. Channel stacking determines the vertical sand connections, especially in the upstream area where channels are less mobile. Therefore, the preferential flow concentrates in the upstream area (Figure 2), and exerts a stronger control on the flow field than horizontal cases, with 40% to 70% of discharge at the fast exit locations (Figure S10c). In muddy deltas (30% ISF), more stable channels with less migration create more vertical connections and preferential flow. Thus, K_{eff}/K_G and T_a/T_5 are both greater for 30% ISF than 50% and 70% ISF conditions (Figure 4 c&d and Figure S10 b&f).

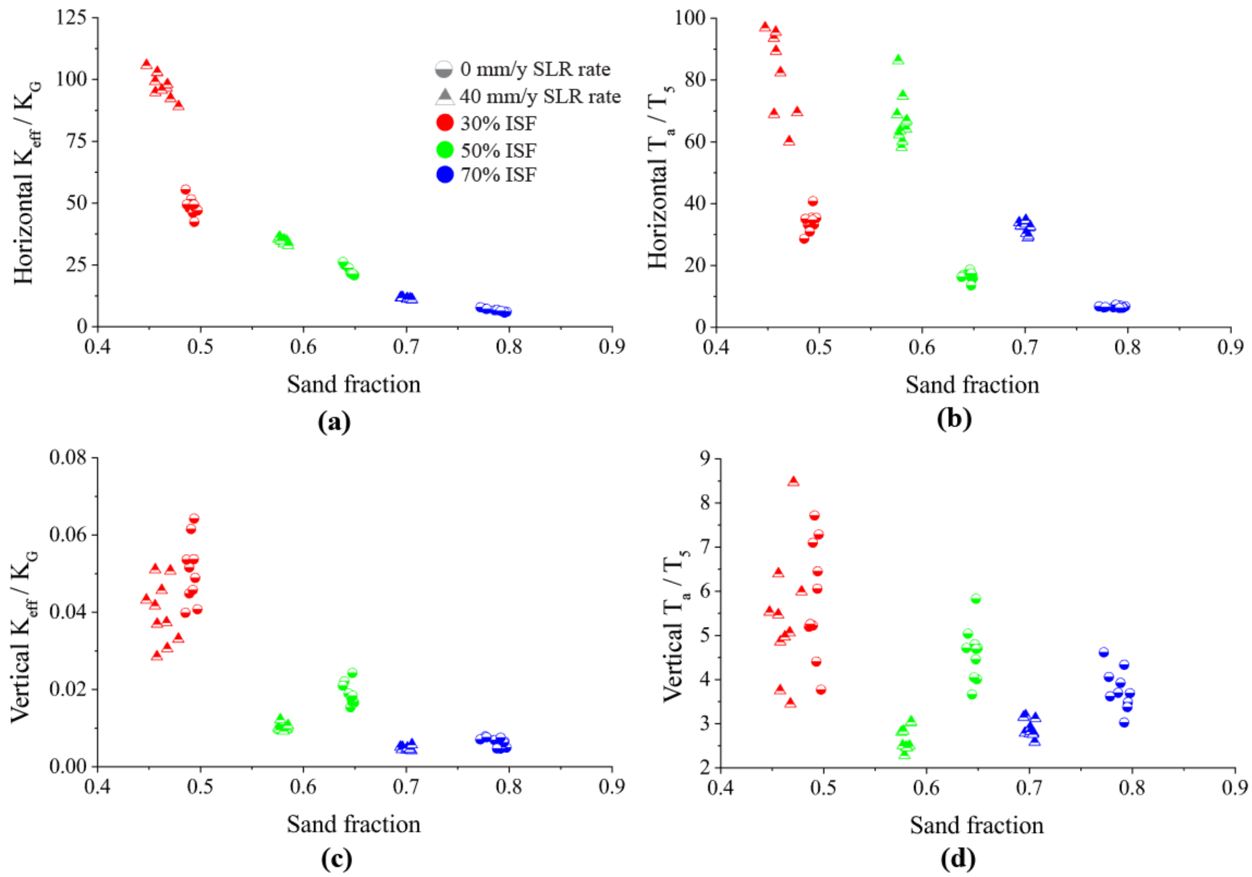

Figure 4. The effect of ISF on normalized dynamic connectivity. (**a**) and (**b**) are horizontal K_{eff}/K_G and T_a/T_5. (**c**) and (**d**) are vertical K_{eff}/K_G and T_a/T_5. Only SLR rates of 0 mm/y and 40 mm/y are shown for clarity while spanning a range of values.

3.3 The effect of the rate of Sea-Level Rise (SLR)

In coastal regions, delta formation is influenced by rate of SLR. The rate of sea-level variation determines the space available for sediment deposition (accommodation), and also influences channel flow via backwater effects. A higher SLR rate has been demonstrated by conceptual models (Jerolmack, 2009) and physical experiments (Martin et al., 2009) to intensify channel branching and shorten the autogenic timescales. This effect was also supported by DeltaRCM numerically (Liang et al., 2016a). In the DeltaRCM simulations, a higher deposition rate on the delta top is required to maintain an elevation of the shoreline close to sea level under higher SLR rates, and river channels split into more distributaries to deliver sediment. Though sand fraction is not strongly influenced by SLR rate, there is a trend of sand fraction decreasing slightly with SLR rates (Figure S8a). This is most likely because high rates of sea-level rise cause more deposition of sand near the sediment source, which is removed when extracting the sub-domain. The effect of SLR rate on horizontal and vertical connectivity is described below. Only the 30% ISF case is discussed here since the effect of SLR rate in other ISF simulations is similar (Figure S8-S10).

In the horizontal plane, normalized dynamic connectivity increases with SLR rates (Figure 5a & b and Figure S9 b&f). A possible explanation is that higher SLR rate results in a lower sand fraction in the main part of the delta, similar to the effect of ISF, thus resulting in greater normalized dynamic connectivity in a system that is always fully percolated. Another explanation is that high SLR rate models have greater horizontal percolation because channels tend to span the formation from upstream to downstream (Figure S2). This results in increasing horizontal preferential flow (L/T_5) with SLR rates (Figure S9d).

In the vertical direction, both sand fraction and channel migration vary with SLR rates, and they have opposing effects on dynamic connectivity, resulting in a lack of systematic variation with SLR rates (Figure 5 c&d and Figure S10 b&f). Higher SLR rate results in a lower sand fraction, which creates more stable channels, resulting in a higher vertical connectivity. On the other hand, fast deposition rates in the high-SLR conditions result in more river avulsions and migration, which reduces the vertical sand connections.

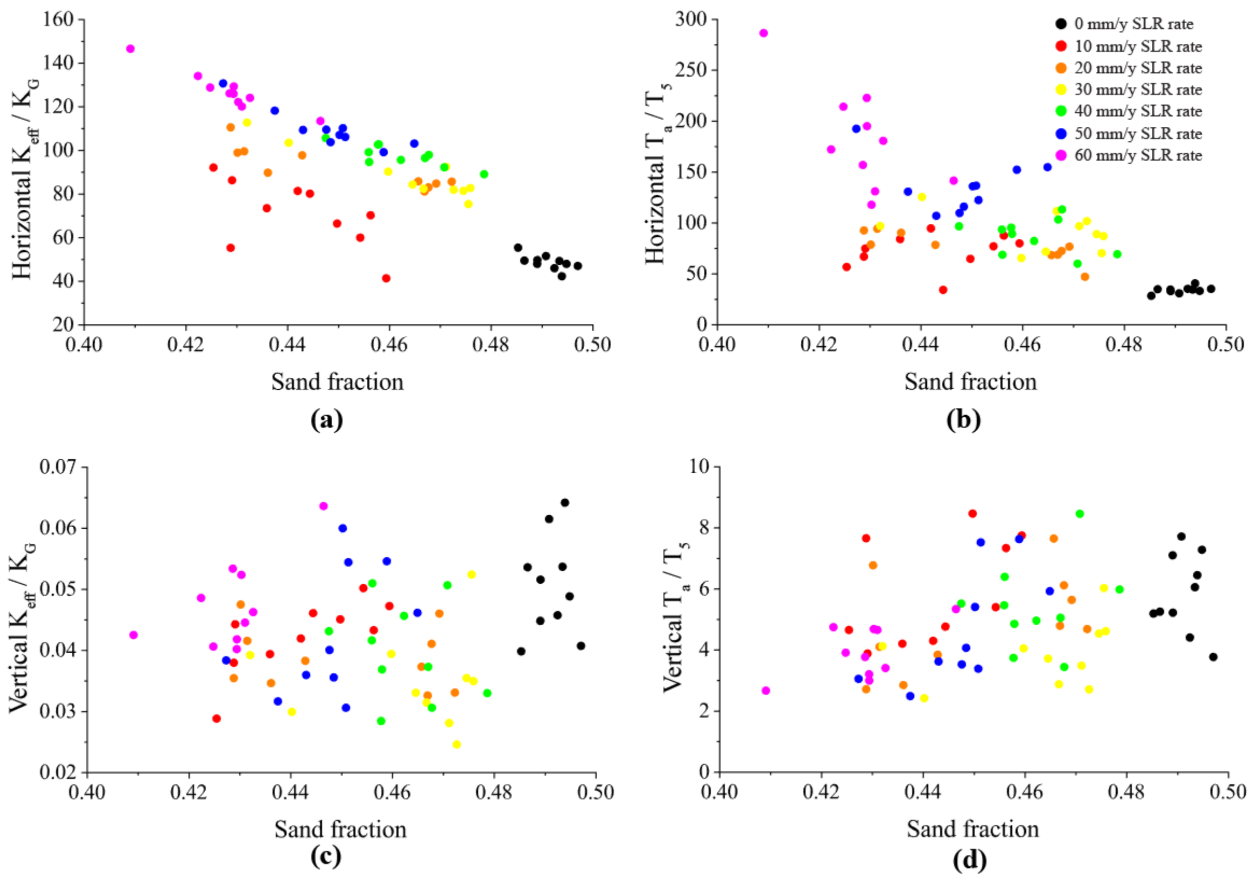

Figure 5. The effect of SLR rates on static and normalized dynamic connectivity, only 30% ISF displayed. (**a**) and (**b**) are horizontal K_{eff}/K_G and T_a/T_5. (**c**) and (**d**) are vertical K_{eff}/K_G and T_a/T_5.

4. Discussion

The selection of connectivity metrics is key in determining the relationship between stratigraphic structure and groundwater flow behavior. 3D static metrics were not distinguish characteristics in many cases because the sand in the simulated systems in this work was found to be highly connected horizontally. Thus, 3D geobody connectivity and percolated path ratio were exactly same and very close to the overall net-to-gross ratio. Statistics in 2D sections, however, proved to be useful in correlating horizontal and vertical dynamic behavior, and performed well in predicting a variety of dynamic metrics, such as K_{eff}, K_{eff}/K_G and L/T_5 (Table 3). The most useful dynamic metrics in this study were K_{eff}/K_G and T_a/T_5. These are higher order metrics normalized by lower order metrics, removing the influence of total sand fraction and indicating spatial connectedness and preferential flow behavior. In addition to the metrics mentioned above, we calculated connectivity metrics which eventually excluded from this paper, such as geodesic distance (Passalacqua et al., 2012), metrics related to the variogram (Western et al., 1998; Kundby & Carrera, 2005), connectivity function (Western et al., 2001), flow channeling (Le Goc et al., 2010), and hydraulic diffusivity (Kundby & Carrera, 2006). These metrics are not presented in this work because they are not well correlated with other metrics or they do not capture the important features of flow and advective transport in a channelized system.

Different static metrics correlate with different dynamic behaviors in the horizontal and vertical directions. In general, 1st-order static metrics have a good correlation with overall flow in the horizontal plane, and 2nd-order static metrics perform well in predicting vertical overall flow and preferential flow (Table 3). Horizontal overall flow is very easy to predict with static metrics and shows agreement among ISF and SLR rates, because the delta system is highly percolated and sand-connected horizontally. However, the horizontal preferential flow is difficult to capture because the system is highly percolated for all conditions, so that fast flow is not sensitive to channel variations in this system. Vertical flow behavior is more complex than horizontal flow (Figure 4c&d, Figure 5c&d) - it is controlled by channel stacking which is influenced by multiple geologic conditions and varies by spatial location. For example, increasing SLR rate produces more channel distributaries and promotes channel migration, while a lower sand fraction for higher SLR rate decreases channel migration (Figure S8a). Additionally, upstream regions have more stable channels than downstream regions. These combined effects make vertical flow concentrate in upstream areas and obscure any relationship to geologic setting.

Our analysis shows that flow and advective transport prediction could be improved by understanding of geologic structure and external forcings of deltaic systems. According to this analysis, lateral flow dynamics, such as submarine groundwater discharge (SGD) and saltwater intrusion (SWI), would occur at high rates even in deltas with rich mud content, due to existing highly percolated channels (e.g., Kolker et al., 2013). The hydrogeologic parameters and hydrochemistry is likely to be strongly heterogeneous in the lower delta plain environments due to sedimentation of complex river distributary networks - this paleo-channel distribution tends to create a multi-facies, inter-fingering architecture (Goodbred & Kuehl, 2000; Goodbred et al., 2003; Hoque et al., 2017). Channel stacking is an important structural factor in this study, and is predictable in the delta evolution process. For example, in the Ganges Delta in the mid-Holocene, sea-level rise and more humid conditions accelerated sediment discharge and river channel migration (Goodbred et al., 2003), so paleo-channels tend to have less stacking and fewer vertical sand connections. However, in the late-Holocene, the stacking density may have increased again due to a less active sedimentary environment. Spatially, greater infiltration and vertical flow may occur in upstream regions due to more consistent channel stacking. This consistent stacking may contribute to vertical transport of contaminants, such as geogenic arsenic in deltas of Southern Asia, from Holocene aquifers to older strata (e.g., Michael & Khan, 2016; Khan et al., 2019).

This study synthetically relates the delta sedimentological structure and flow behaviors. In order to extend the relationship to real deltas, several factors should be considered. First, the external forcings (ISF and SLR rate) are held constant in our simulations, whereas forcing in real deltas is variable. This may limit the sedimentary time interval over which insights from knowledge of forcing may be applied to the subsurface. We also do not consider forcing mechanisms such as tidal effects in this study. Tides act as pistons pushing channel water back, interacting with both fluvial and ocean material (Ensign et al., 2015). This may influence both sediment distribution and river morphology, changing the channel distributions and preservation in the downstream region.

This work shows the strong influence of subsurface channel structure on groundwater flow and advective solute transport dynamics. Because these structures, primarily sandy channels, are a result of deposition by river channels on land surface, there is potential to predict flow and transport based on surface drainage network characteristics. Subsurface information acquisition including static and dynamic data are costly, while surface information is more easily obtained. In our companion paper (Hariharan et al., submitted), we show that the depositional environment affects surface metrics of shoreline roughness and wetted fraction, which are in turn indicative of subsurface static metrics, such as connectivity and percolated path ratio. Thus, information on subsurface structure can be obtained from surface information and understanding of the external forcings. Here we show that these subsurface static metrics also are predictive of flow and advective transport behavior. This connection, from surface to subsurface to flow and transport, has the potential to greatly improve our ability to predict vulnerability of groundwater resources to contamination in globally important deltaic aquifer systems.

5. Conclusions

This study aims to investigate the relationship between flow behavior and geologic structure in deltaic aquifers, and the influence of external forcings. We establish the links between static and dynamic connectivity in synthetic systems generated with different rates of sea-level rise and sand proportion to gain insights into how geologic features and external forcings can help to predict groundwater flow and advective transport behavior. In general, static metrics are more correlated to flow metrics than to transport metrics, and the metrics for horizontal flow are better correlated with static metrics. The results show that the net-to-gross ratio and spatial connections capture the overall flow in the horizontal direction, while spatial connectivity and channel stacking capture the vertical flow behavior. Horizontal flow behavior is well predicted by lower-order static metrics because the flow systems are horizontally percolated. Vertical flow and transport behavior is controlled by higher-order static metrics due to less channel connectedness.

We also show the effect of ISF and SLR rate on the numerically simulated hydraulic connectivity of delta settings. Different ISF and SLR rate yield different geologic structure and channel variation, thus influencing horizontal and vertical flow. The main findings are:

1) Horizontal normalized dynamic connectivity is greater in low-ISF deltas because the systems are still percolated, but with less sand. This indicates that processes dependent on horizontal flow and transport in deltas, such as contamination by lateral seawater intrusion or submarine groundwater discharge, still occur in muddy deltas, but with more dominant preferential flow. This has implications for the rate of intrusion, for example, because transport in a more highly preferential system occurs faster for the same hydraulic gradient. It also has

implications for prediction of contamination pathways, because more preferential systems are more highly variable, thus monitoring and managing can be more difficult (e.g., Yu and Michael, 2019; Geng and Michael, 2020).

2) Vertical normalized dynamic connectivity is also greater with less sand input because channels in muddy systems tend to migrate less, thus channel stacking creates greater vertical connectedness. This implies that muddy deltas, despite having more low-permeability sediments that may be considered protective, may actually be more vulnerable to vertical contaminant transport, such as arsenic in shallow aquifers (e.g., Fendorf et al., 2010) and salt from surface sources such as storm-surge overwash (e.g., Mahmoodzadeh and Karamouz, 2019).

3) Higher rates of SLR increase horizontal connectivity by creating a more percolated structure horizontally, while vertical flow and channel stacking patterns are too complex to vary systematically with SLR rate. Thus, understanding of SLR rate during delta formation may improve predictability of horizontal processes, such as seawater intrusion and submarine groundwater discharge, as indicated above, but it is a less useful predictor for vertical flow and transport processes.

These insights illustrate the potential to improve prediction of groundwater flow and solute transport behavior through analysis of geological architecture and understanding of external forcings in deltaic aquifers. In combination with Hariharan et al. (submitted), these insights also form a basis for further study of the translation of delta surface characteristics to groundwater flow and solute transport processes.

Acknowledgements

The authors acknowledge support from the National Science Foundation via EAR-1719670/EAR-1719638. The DeltaRCM model can be downloaded from the CSDMS model repository at https:// csdms.colorado.edu/wiki/Model:DeltaRCM. Example MODFLOW and MODPATH input files are given in the supplementary material.

References

Barlow, J.R.B., & Clark, B.R. (2011). *Simulation of water-use conservation scenarios for the Mississippi Delta using an existing regional groundwater flow model*. Reston, VA: USGS, Scientific Investigation Report 2011-5019. https://doi.org/10.3133/sir20115019

Basu, A.R., Jacobsen, S.B., Poreda, R.J., Dowling, C.B., & Aggarwal PK (2001). Large Groundwater Strontium Flux to the Oceans from the Bengal Basin and the Marine Strontium Isotope Record. *Science*, 293: 1470-1473. doi: 10.1126/science.1060524

Bhattacharyya, P., Bhattacharya, J.P., & Khan, S.D. (2015). Paleo-channel reconstruction and grain size variability in fluvial deposits, Ferron Sandstone, Notom Delta, Hanksville, Utah. *Sedimentary Geology*, 325, 17–25. https://doi.org/10.1016/j.sedgeo.2015.05.001

Bianchi, M., Zheng, C., Wilson, C., Tick, G.R., Liu, & G., Gorelick, S.M. (2011). Spatial connectivity in a highly heterogeneous aquifer: From cores to preferential flow paths. *Water Resources Research*, 47, W05524. https://doi.org/10.1029/2009WR008966

Cazenave, A., Dieng, H.B., Meyssignac, B., von Schuckmann, K., Decharme, B., & Berthier, E. (2014). The rate of sea-level rise. *Nature Climate Change*. doi: 10.1038/NCLIMATE2159.

Dagan, G. (1986). Statistical theory of groundwater flow and transport: pore to laboratory, laboratory to formation, and formation to regional scale. *Water Resources Research*, 22(9):120S–34S. https://doi.org/10.1029/WR022i09Sp0120S

Dagan, G., Fiori, A., & Jankovic, I. (2003). Flow and transport in highly heterogeneous formations: 1. Conceptual framework and validity of first-order approximations. *Water Resources Research*, 39(9). 1268. https://doi.org/10.1029/2002WR001717

Devlin, J.F. (2015). HydrogeoSieveXL: an Excel-based tool to estimate hydraulic conductivity from grain-size analysis. *Hydrogeology Journal*, 23: 837-844. https://doi.org/10.1007/s10040-015-1255-0

Efros, A.A., & Freeman, W.T. (2001). Image quilting for texture synthesis and transfer. In *Proceedings of the 28th annual conference on computer graphics and interactive techniques, siggraph 2001* (pp. 341-346). New York, NY, USA: ACM Press.

Ensign, S.H., Noe, G.B., Hupp, C.R., Skalak, K.J. (2015). Head-of-tide bottleneck of particulate material transport from watersheds to estuaries. *Geophysical Research Letters*, 42, 10671-10679. doi:10.1002/2015GL066830

Erban, L.E., Gorelick, S.M., Zebker, H.A., & Fendorf, S. (2013). Release of arsenic to deep groundwater in the Mekong Delta, Vietnam, linked to pumping-induced land subsidence. *Proceedings of the National Academy of Sciences of the United States of America*, 110(34): 13751-13756. https://doi.org/10.1073/pnas.1300503 110

Feirstein, E.J., Zamora, F., Vionnet, L.B., & Maddock, T. (2008). *Simulation of groundwater conditions in the Colorado River Delta, Mexico*. Tucson, AZ.

Fendorf, S.F., Michael, H.A., & van Geen, A. (2010). Factors controlling the spatial and temporal variations of arsenic in groundwater of South and Southeast Asia. *Science*, 328, 1123-1127, doi: 10.1126/science.1172974.

Frippiat, C.C., Illangasekare, T.H., & Zyvoloski, G.A. (2009). Anisotropic effective medium solutions of head and velocity variance to quantify flow connectivity. *Advances in Water Resources*, 32(2):239–49. https://doi.org/10.1016/j.advwatres.2008.11.001

Gelhar, L.W. (1986). Stochastic subsurface hydrology: from theory to applications. *Water Resources Research*, 22(9):135S–45S. https://doi.org/10.1029/WR022i09Sp0135S

Geng, X., & Michael, H.A. (2020). Preferential flow enhances pumping ‐ induced saltwater intrusion in volcanic aquifers. *Water Resources Research*, 56, e2019WR026390. https://doi.org/10.1029/2019WR026390

Gilbert, G. (1885). *The topographic features of lake shores*. Washington, D.C.: US Geological Survey Annual Report, Department of Interior,

Goodbred, S.L., & Kuehl, S.A. (2000). The significance of large sediment supply, active tectonism, and eustasy on margin sequence development: Late Quaternary stratigraphy and evolution of the Ganges–Brahmaputra delta. *Sedimentary Geology*, 133, 227-248. https://doi.org/10.1016/S0037-0738(00)00041-5

Goodbred, S.L., Kuehl, S.A., Steckler, M.S., & Sarker, M.H. (2003). Controls on facies distribution and stratigraphic preservation in the Ganges–Brahmaputra delta sequence. *Sedimentary Geology*, 155, 301-316. https://doi.org/10.1016/S0037-0738(02)00184-7

Guo, W., & Langevin, C. (2002). *User's guide to SEWAT: a computer program for simulation of three-dimensional variable-density ground-water flow*. USGS report. https://doi.org/10.3133/twri06A7

Guswa, A.J., & Freyberg, D.L. (2002). On using the equivalent conductivity to characterize solute spreading in environments with low-permeability lenses. *Water Resources Research*, 30(8):11-32. https://doi.org/10.1029/2001WR000528

Harbaugh, A.W. (2005). *MODFLOW-2005, the US Geological Survey modular ground-water model: the ground-water flow process*. USGS report. https://doi.org/10.3133/tm6A16

Hariharan, J., Xu, Z., Michael, H.A., Paola, C., Steel, E., & Passalacqua, P. (submitted). Constraining subsurface properties from surface information in river deltas - part 1: relating surface and subsurface geometries. Submitted to *Water Resources Research*.

Heller, P.L., Paola, C., Hwang, I.G., John, B., & Steel, R. (2001). Geomorphology and sequence stratigraphy due to slow and rapid base-level changes in an experimental subsiding basin (XES 96–1). AAPG Bull., 85(5). 817–838. doi: 10.1306/8626CA0F-173B-11D7-8645000102C1865D

Hiatt, M., & Passalacqua, P. (2015). Hydrological connectivity in river deltas: The first-order importance of channel-island exchange. *Water Resources Research*, 51, 2264–2282. https://doi.org/10.1002/2014WR016149

Hovadik, J.M., & Larue, D.K. (2007). Static characterizations of reservoirs: refining the concepts of connectivity and continuity. *Petroleum Geoscience*, 13(3):195–211. https://doi.org/10.1144/1354-079305-697

Hoque, M.A., Burgess, W.G., & Ahmed, K.M. (2017). Integration of aquifer geology, groundwater flow and arsenic distribution in deltaic aquifers – A unifying concept. *Hydrological Processes*, 31: 2095–2109. https://doi.org/10.1002/hyp.11181

Jankovic, I., Maghrebi, M., Fiori, A., & Degan, G. (2017). When good statistical models of aquifer heterogeneity go right: The impact of aquifer permeability structures on 3D flow and transport. *Advances in Water Resources*, 100: 199-211. https://doi.org/10.1016/j.advwatres.2016.10.024

Jerolmack, D.J. (2009). Conceptual framework for assessing the response of delta channel networks to Holocene sea level rise. *Quaternary Science Reviews*, 28(17–18): 1786–1800. https://doi.org/10.1016/j.quascirev.2009.02.015

Jessen, S., Larsen, F., Postma, D., Viet, P.H., Ha, N.T., & Nhan, P.Q., et al. (2008). Palaeo-hydrogeological control on groundwater As levels in Red River delta, Vietnam. *Applied Geochemistry*, 23, 3116-3126. https://doi.org/10.1016/j.apgeochem.2008.06.015

Khan, M.R., Koneshloo, M., Knappett P.S.K., Ahmed, K.M., Bostick, B.C., & Mailloux B.J., et al. (2016). Megacity pumping and preferential flow threaten groundwater quality. *Nature Communications*, 7: 12833. doi: 10.1038/ncomms12833

Khan, M.R., Michael, H.A., Nath, B., Huhmann, B.L., Harvey, C.F., & Mukherjee, A., et al. (2019). High‐arsenic groundwater in the southwestern Bengal Basin caused by a lithologically controlled deep flow system. *Geophysical Research Letters*, 46, 13062–13071. https://doi.org/10.1029/2019GL084767

Kim, W., Paola, C., Swenson, J.B., & Voller, V.R. (2006). Shoreline response to autogenic processes of sediment storage and release in the fluvial system. *Journal of Geophysical Research: Earth Surface*, 111(F4). F04013. https://doi.org/10.1029/2006JF000470

Krishnan, S., & Journel, A.G. (2003). Spatial connectivity: From variograms to multiple-point measures. *Mathematical Geology*, 35(8). 915–925.

Kolker, A.S., Cable, J.E., Johannesson, K.H., Allison, M.A., & Inniss, L.V. (2013). Pathways and processes associated with the transport of groundwater in deltaic systems. *Journal of Hydrology*, 498, 319–334. https://doi.org/10.1016/j.jhydrol.2013.06.014

Kundby, C., & Carrera, J. (2005). On the relationship between indicators of geostatistical, flow and transport connectivity. *Advances in Water Resources*, 28: 405–421. https://doi.org/10.1016/j.advwatres.2004.09.001

Kundby, C., & Carrera, J. (2006). On the use of apparent hydraulic diffusivity as an indicator of connectivity. *Journal of Hydrology*, 329: 377-389. https://doi.org/10.1016/j.jhydrol.2006.02.026

Larsen, F., Tran, L.V., Hoang, H.V., Tran, L.T., Christiansen, A.V., & Pham, N.Q. (2017). Groundwater salinity influenced by Holocene seawater trapped in incised valleys in the Red River delta plain. *Nature Geoscience*, 10, 376-381.

Larue, D.K., & Hovadik, J. (2006). Connectivity of channelized reservoirs: a modelling approach. *Petroleum Geoscience*, 12(4):291–308. https://doi.org/10.1144/1354-079306-699

Le Goc, R., de Dreuzy, J.R., Davy, P. (2010). Statistical characteristics of flow as indicators of channeling in heterogeneous porous and fractured media. *Advances in Water Resources*, 33(3):257–69. https://doi.org/10.1016/j.advwatres.2009.12.002

Liang, M., Voller, V.R., Paola, C. (2015a). A reduced-complexity model for river delta formation - Part 1: Modeling deltas with channel dynamics. *Earth Surface Dynamics*, 3: 67–86. https://doi.org/10.5194/esurf-3-67-2015

Liang, M., Geleynse, N., Edmonds, D.A., & Passalacqua, P. (2015b). A reduced-complexity model for river delta formation - Part 2: Assessment of the flow routing scheme. *Earth Surface Dynamics*, 3: 87–104. https://doi.org/10.5194/esurf-3-87-2015

Liang, M., Dyk, C.V., & Passalacqua, P. (2016a). Quantifying the patterns and dynamics of river deltas under conditions of steady forcing and relative sea level rise, *Journal of Geophysical Research: Earth Surface*, 121: 465–496. https://doi.org/10.1002/2015JF003653

Liang, M., Kim, W., & Passalacqua, P. (2016b). How much subsidence is enough to change the morphology of river deltas? *Geophysical Research Letters*, 43. https://doi.org/10.1002/2016GL070519

Madden, T.R. (1983). Microcrack connectivity in rocks - a renormalization-group approach to the critical phenomena of conduction and failure in crystalline rocks. *Journal of Geophysical Research: Solid Earth*, 88(NB1):585–92. https://doi.org/10.1029/JB088iB01p00585

Mahmoodzadeh, D., & Karamouz, M. (2019). Seawater intrusion in heterogeneous coastal aquifers under flooding events. *Journal of Hydrology*, 568, 1118-1130. https://doi.org/10.1016/j.jhy drol.2018.11.012

Martin, J., Sheets, B., Paola, C., Hoyal, D. (2009). Influence of steady base-level rise on channel mobility, shoreline migration, and scaling properties of a cohesive experimental delta. *Journal of Geophysical Research: Earth Surface*, 114, F03017. https://doi.org/10.1029/2008JF001142

Matheron, G. (1967). Composition des perméabilités en milieu poreux hétérogène: méthode de Schwydler et règles de pondération. *Revue DE L'Institut Francais DU Petrole*, 23:443–66.

Miall, A.D. (2014). *Fluvial depositional systems*. New York, NY: Springer.

de Marsily, G. (1985). Flow and transport in fractured rocks: connectivity and scale effect. In: International Association of Hydrogeologists (Eds.), *Hydrogeology of rocks of low permeability* (Vol. 17, pp. 267-277). Tucson, AZ.

Michael, H.A., & Voss, C.I. (2008). Evaluation of the sustainability of deep groundwater as an arsenic-safe resource in the Bengal Basin. *Proceedings of the National Academy of Sciences of the United States of America*, 105(25): 8531-8536. https://doi.org/10.1073/pnas.0710477105

Michael, H.A., & Voss, C.I. (2009). Controls on groundwater flow in the Bengal Basin of India and Bangladesh: regional modeling analysis. *Hydrogeology Journal*, 17: 1561-1577.

Michael, H.A., Scott, K.C., Koneshloo, M., Yu, X., Khan, M.R., & Li, K. (2016). Geologic influence on groundwater salinity drives large seawater circulation through the continental shelf. *Geophysical Research Letters*, 43. https://doi.org/10.1002/2016GL070863

Michael, H.A. & Khan, M.R. (2016). Impacts of physical and chemical aquifer heterogeneity on basin-scale solute transport: Vulnerability of deep groundwater to arsenic contamination in Bangladesh. *Advances in Water Resources*, 98, 147-158. https://doi.org/10.1016/j.advwatres.2016.10.010

Mohammed, K., Ramirez-Hernadez, J., & Sheng, Z. (2017). Surface and groundwater flow modeling for calibrating steady state using MODFLOW in Colorado River Delta, Baja California, Mexico. *Modeling Earth Systems and Environment*, 3, 815-824.

Overeem, I., & Syvitski, J.P.M. (2009). Dynamics and Vulnerability of Delta Systems. *LOICZ Reports & Studies*, No. 35. GKSS Research Center.

Passalacqua, P., Belmont, P., Foufoula-Georiou, F. (2012). Automatic geomorphic feature extraction from lidar in flat and engineered landscapes. *Water Resources Research*, 48, W03528. https://doi.org/10.1029/2011WR010958

Pollock, D.W. (2016). *User guide for MODPATH Version 7 - A particle-tracking model for MODFLOW*. Reston VA: USGS report. http://dx.doi.org/10.3133/ofr20161086.

Rao, S.V.N., Bhallamudi, S.M., Thandaveswara, B.S., & Sreenivasulu, V. (2005). Planning Groundwater Development in Coastal Deltas with Paleo Channels. *Water Resources Management*, 19: 625–639.

Reitz, M.D., Pickering, J.L., Goodbred, S.L., Paola, C., Steckler, M.S., Seeber, L., Akhter, S.H. (2015). Effects of tectonic deformation and sea level on river path selection: Theory and application to the Ganges-Brahmaputra-Meghna River Delta, *Journal of Geophysical Research: Earth Surface*, 120(4). 671–689. https://doi.org/10.1002/2014JF003202

Renard, P., Allard, D. (2013). Connectivity metrics for subsurface flow and transport. *Advances in Water Resources*, 51: 168-196. https://doi.org/10.1016/j.advwatres.2011.12.001

Spratt, R.M., & Lisiecki, L.E. (2016). A Late Pleistocene sea level stack. *Climate of the Past*, 12(4), 1079–1092. https://doi.org/10.5194/cp-12-1079-2016

Tessler, Z.D., Vörösmarty, C.J., Grossberg, M., Gladkova, I., Aizenman, H., Syvitski, J.M.P., & Foufoula-Georgiou, E. (2015). Profiling risk and sustainability in coastal deltas of the world. *Science*, 349 (6248). 638-643. doi: 10.1126/science.aab3574

Sanchez-Vila, X., Carrera, J., & Girardi, J.P. (1996). Scale effects in transmissivity. *Journal of Hydrology*, 183:1–22.

Sawyer A.H., Edmonds, D.A., & Knights, D. (2015). Surface water-groundwater connectivity in deltaic distributary channel networks. *Geophysical Research Letters*, 42, 10, 10299-10306. doi:10.1002/2015GL066156

Shamsudduha, M., Taylor, R.G., Ahmed, K.M., & Zahid, A. (2011). The impact of intensive groundwater abstraction on recharge to a shallow regional aquifer system: evidence from Bangladesh. *Hydrogeology Journal*, 19: 901–916.

Shaw, J.B., Mohrig, D., & Whitman, S.K. (2013). The morphology and evolution of channels on the Wax Lake Delta, Louisiana, USA. *Journal of Geophysical Research: Earth Surface*, 118, 1562-1584. https://doi.org/10.1002/jgrf.20123

Sheets, B.A., Hickson, T.A. & Paola, C. (2002). Assembling the stratigraphic record: Depositional patterns and time-scales in an experimental alluvial basin. *Basin Research*, 14(3). 287–301. https://doi.org/10.1046/j.1365-2117.2002.00185.x

Stauffer, D., & Aharony, A. (2014). *Introduction to percolation theory: revised second edition*. London, UK: Taylor and Francis. https://doi.org/10.1201/9781315274386

Straub, K.M., Paola, C., Mohrig, M., Wolinsky, M.A., George, T. (2009). Compensational stacking of channelized sedimentary deposits. *Journal of Sedimentary Research*, 79, 673–688. doi: 10.2110/jsr.2009.070

Syvitski, J.P.M., & Saito, Y. (2007). Morphodynamics of deltas under the influence of humans. *Global and Planetary Change*, 57(3–4). 261–282. https://doi.org/10.1016/j.gloplacha.2006.12.001

Syvitski, J.P.M., Kettner, A.J., Overeem, I., Hutton, E.H.W., Hannon, M.T., & Brakenridge, G.R., et al. (2009). Sinking deltas due to human activities. *Nature Geoscience*, 2, 681-686.

van Engelen, J., Verkaik, J., King, J., Nofal, E.R., Bierkens, M.F.P. & Essink, G.H.P.O. (2019). A three-dimensional palaeohydrogeological reconstruction of the groundwater salinity distribution in the Nile Delta Aquifer. *Hydrology and Earth System Sciences*, 23, 5175–5198.

van Geen, A., Zheng, Y., Goodbred, J., Horneman, A., Aziz, Z., & Cheng, Z., et al. (2008). Flushing history as a hydrogeological control on the regional distribution of arsenic in shallow groundwater of the Bengal basin. *Environmental Science & Technology*, 42, 2283-2288. doi: 10.1021/es702316k.

Vukovic, M., & Soro, A. (1992). Determination of hydraulic conductivity of porous media from grain-size composition. *Water Resources Publications*, Littleton, Colorado, USA, 83pp.

Wada, Y., van Beek L.P.H., van Kempen, C.M., Reckman, J.W.T.M., Vasak, S., & Bierkens, M.F.P. (2010). Global depletion of groundwater resources. *Geophysical Research Letters*, 37, L20402. https://doi.org/10.1029/2010GL044571

Wen, X.H., & Gomez-Hernandez, J.J. (1998). Numerical modeling of macrodispersion in heterogeneous media: a comparison of multi-Gaussian and non-multi-Gaussian models. *Journal of Contaminant Hydrology*, 30, 129-156. https://doi.org/10.1016/S0169-7722(97)00035-1

Western, A.W., Blöschl, G., & Grayso, R.B. (1998). How well do indicator variograms capture the spatial connectivity of soil moisture? *Hydrological Processes*, 12, 1851-1868. https://doi.org/10.1002/(SICI)1099-1085(19981015)12:12<1851::AID-HYP670>3.0.CO;2-P

Western, A.W., Blöschl, G., & Grayso, R.B. (2001). Toward capturing hydrologically significant connectivity in spatial patterns. *Water Resources Research*, 37(1): 83-97. https://doi.org/10.1029/2000WR900241

Yu, X., & Michael, H.A. (2019). Mechanisms, configuration typology, and vulnerability of pumping-induced seawater intrusion in heterogeneous aquifers. *Advances in Water Resources*, 128, 117-128. https://doi.org/10.1016/j.advwatres.2019.04.013

Zarlenga, A., Jankovic, I., Fiori, A., & Dagan, G. (2018). Effective Hydraulic Conductivity of Three-Dimensional Heterogeneous Formations of Lognormal Permeability Distribution: The Impact of Connectivity. *Water Resources Research*, 54, 2480–2486. https://doi.org/10.1002/2017WR022141

Zinn, B., & Harvey, C.F. (2003). When good statistical models of aquifer heterogeneity go bad: a comparison of flow, dispersion, and mass transfer in connected and multivariate Gaussian hydraulic conductivity fields. *Water Resources Research*, 39(3): 1051. https://doi.org/10.1029/2001WR001146

Figure 1.

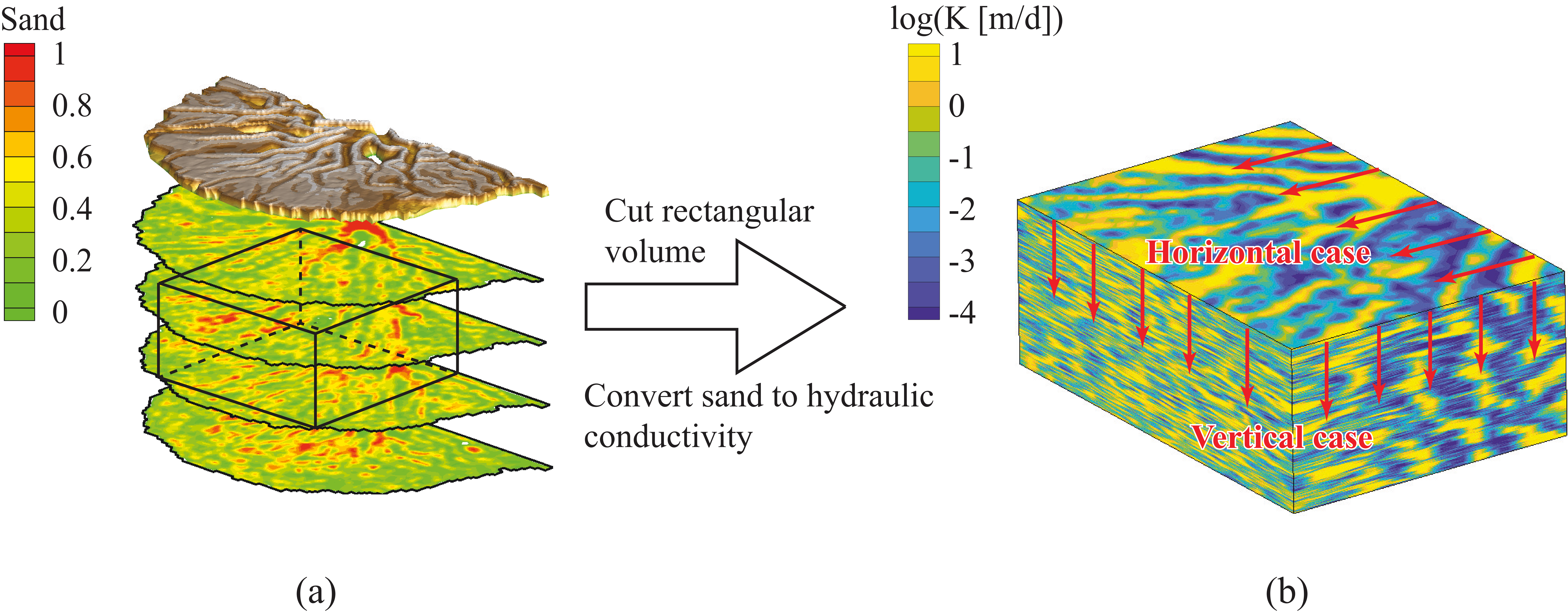

Sand
1
0.8
0.6
0.4
0.2
0
Cut rectangular volume
Convert sand to hydraulic conductivity
log(K [m/d])
1
0
-1
-2
-3
-4
Horizontal case
Vertical case
(a)
(b)

Figure 2.

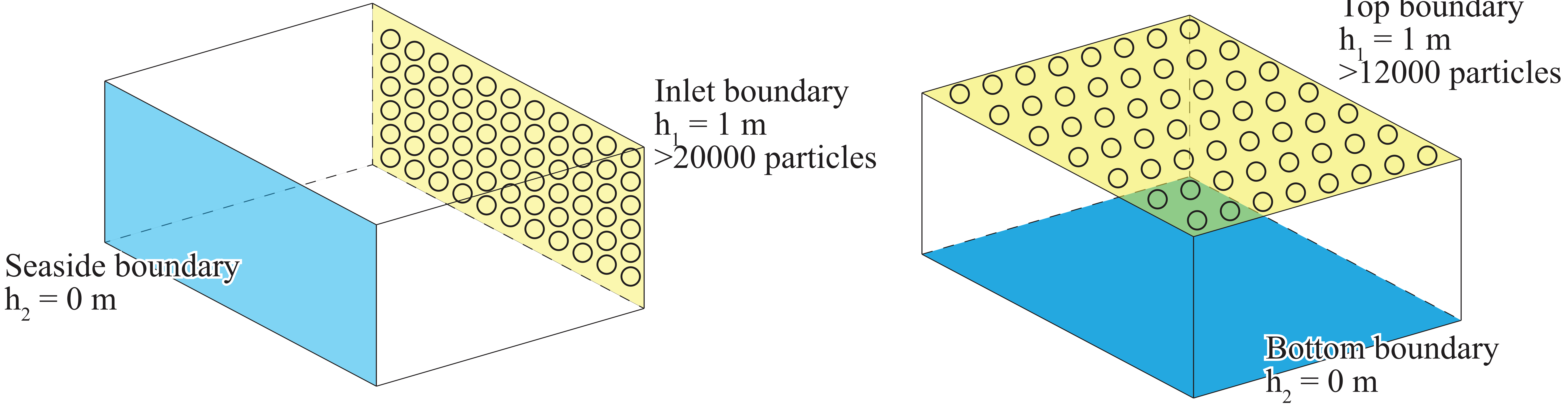

(a) Horizontal case (b) Vertical case

Figure 3.

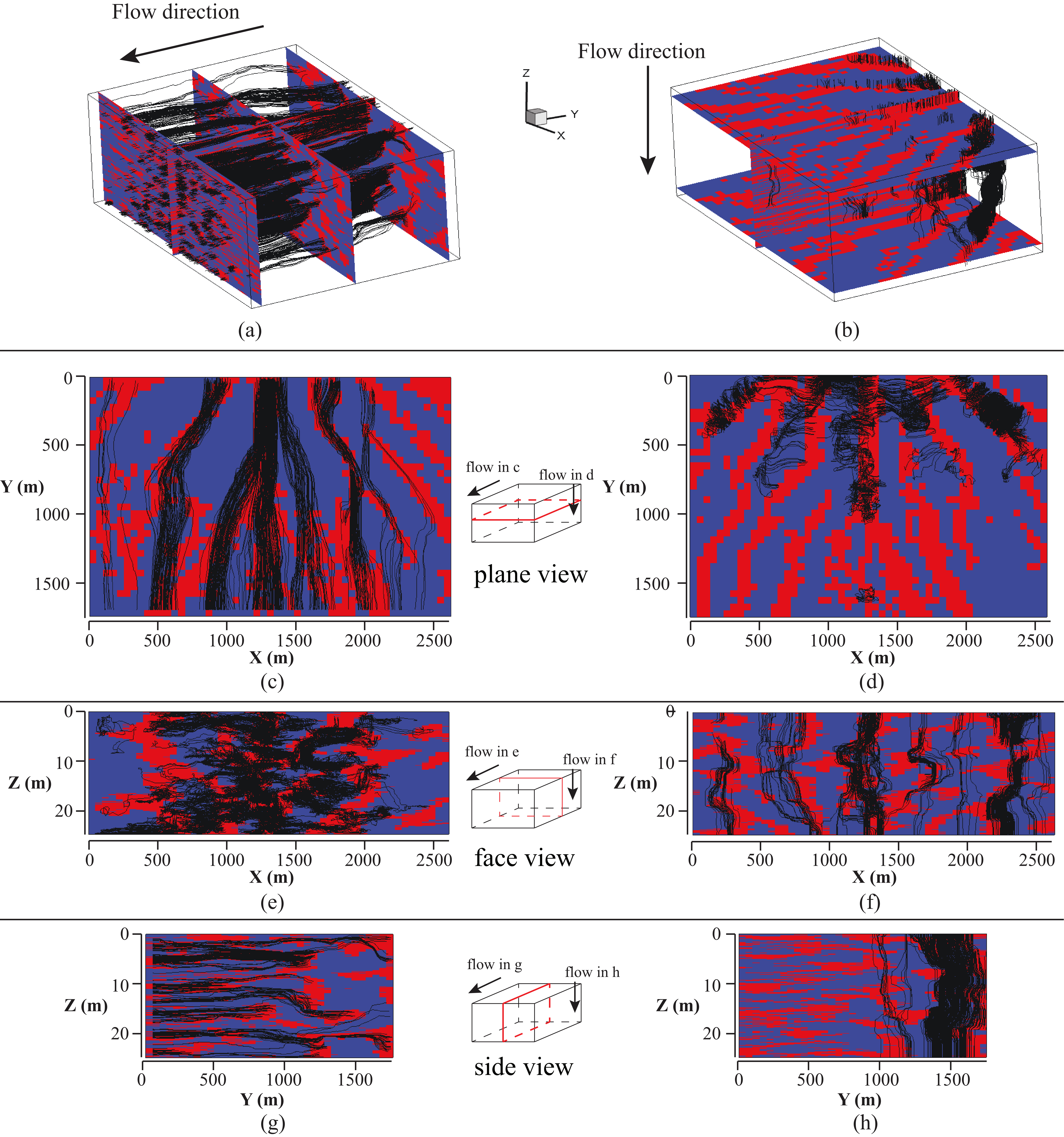

Flow direction
Flow direction
Z
Y
X
(a)
(b)
Y (m)
X (m)
flow in c
flow in d
plane view
(c)
(d)
Z (m)
X (m)
flow in e
flow in f
face view
(e)
(f)
Z (m)
Y (m)
flow in g
flow in h
side view
(g)
(h)

Figure 4.

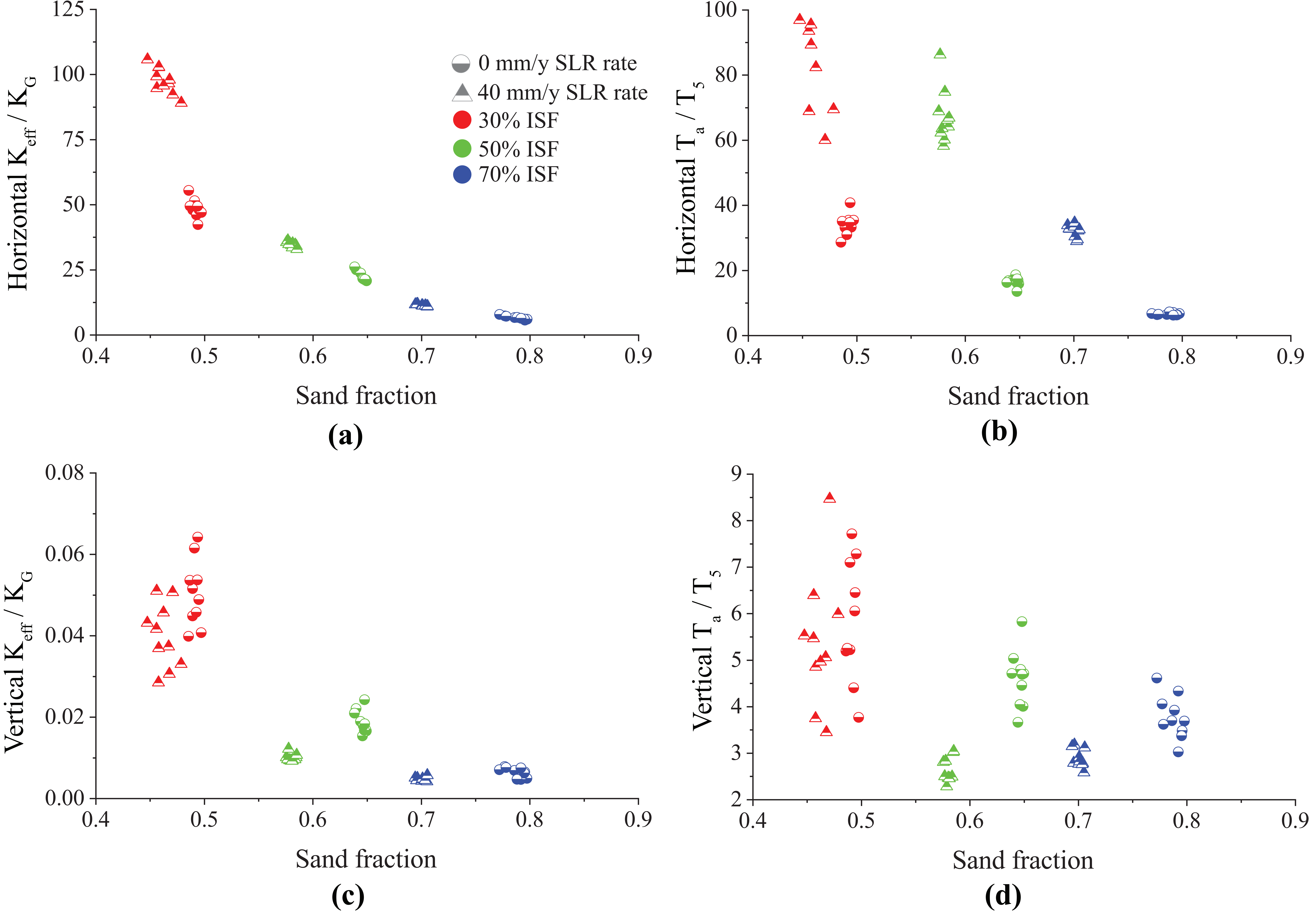
0 mm/y SLR rate
40 mm/y SLR rate
30% ISF
50% ISF
70% ISF
Horizontal K_{eff} / K_G
Sand fraction
(a)
Horizontal T_a / T_5
Sand fraction
(b)
Vertical K_{eff} / K_G
Sand fraction
(c)
Vertical T_a / T_5
Sand fraction
(d)

Figure 5.

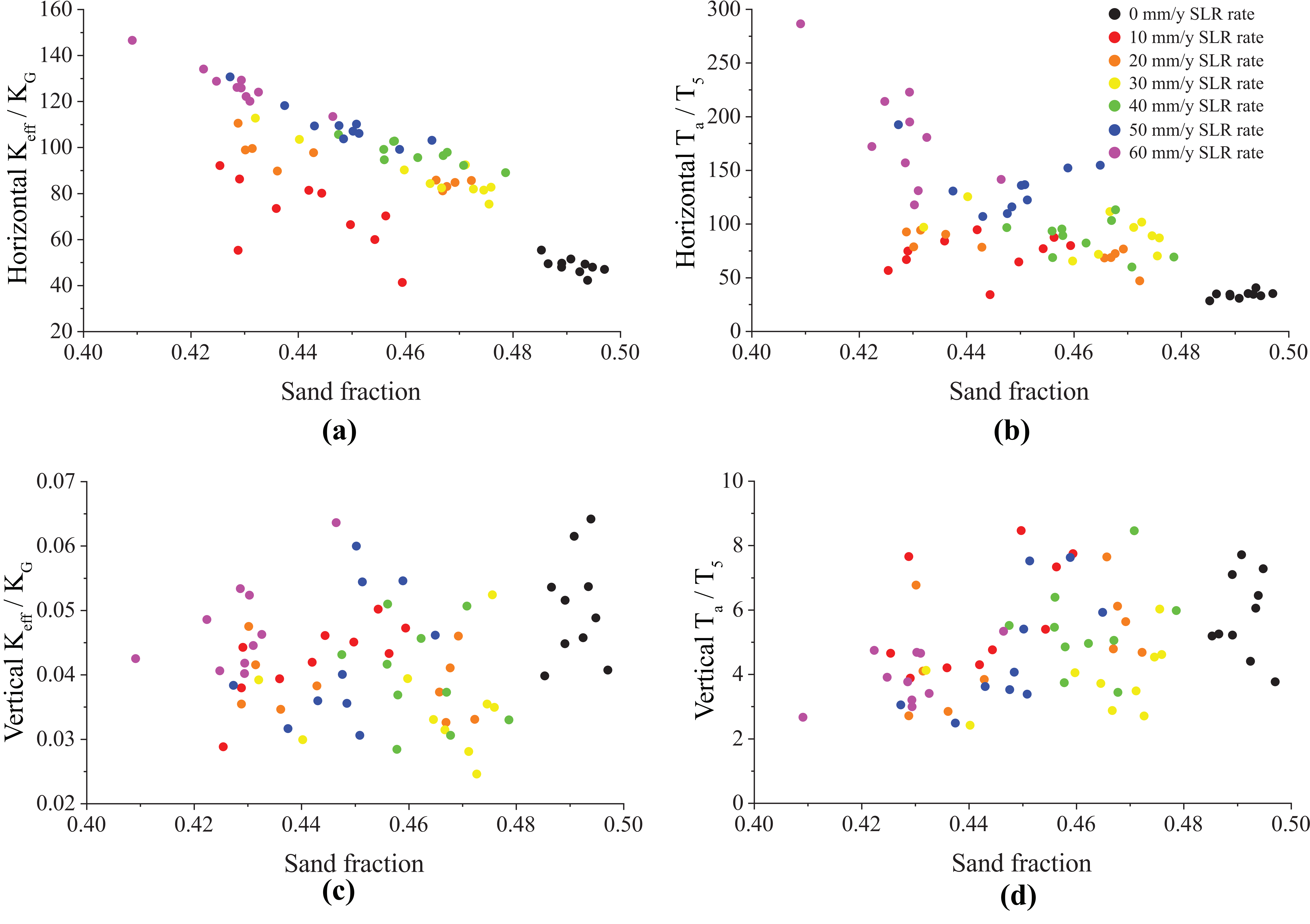

0 mm/y SLR rate
10 mm/y SLR rate
20 mm/y SLR rate
30 mm/y SLR rate
40 mm/y SLR rate
50 mm/y SLR rate
60 mm/y SLR rate
Horizontal K_{eff} / K_G
Horizontal T_a / T_5
Vertical K_{eff} / K_G
Vertical T_a / T_5
Sand fraction
(a)
(b)
(c)
(d)